UNIVERSITY OF GOTHENBURG

THE SAHLGRENSKA ACADEMY

EVALUATION OF ELEGP COLLIMATOR WITH RESOLUTION RECOVERY FOR SPECT/CT

André Lundin

Essay/Thesis:	30 hp
Program and/or course:	Medical Physics Program
Level:	Second Cycle
Semester/year:	At/2015
Supervisor:	Johanna Dalmo, Jakob Himmelman
Examiner:	Magnus Båth
Report no:	

Abstract

Essay/Thesis:	30 hp
Program and/or course:	Medical Physics Program
Level:	Second Cycle
Semester/year:	At/2015
Supervisor:	Johanna Dalmo, Jakob Himmelman
Examiner:	Magnus Båth
Report No:	
Keyword:	Nuclear medicine, contrast, noise, SNR, ^{99m}Tc, ^{111}In, ^{123}I, ^{177}Lu

Purpose: The purpose of this study was to evaluate the extended low energy general purpose (ELEGP) collimator for single photon emission computed tomography (SPECT) with resolution recovery and compare it to the traditionally used collimator for four different radionuclides; ^{99m}Tc, ^{111}In, ^{123}I and ^{177}Lu.

Theory: A relatively new parallel hole collimator; the ELEGP collimator has been created by GE Healthcare, which has larger collimator holes compared to other low energy collimators. The ELEGP collimator has higher sensitivity, but lower resolution. The ELEGP collimator also has a thicker septum, which gives it the ability to image radionuclide distributions emitting gamma with higher energy without septum penetration.
The limited resolution in the collimator means that the images created with ELEGP will have lower spatial resolution, compared to images created with other low energy collimators. According to the manufacturer, the spatial resolution in SPECT images can be compensated for by using the modern reconstruction algorithm Resolution Recovery (RR). This has been shown for Octreoscan® with ^{111}In for liver tumours, which indicates that the ELEGP collimator could be a better choice.
If the ELEGP collimator could be proven to produce images with both lower noise levels and an acceptable spatial resolution and contrast, hospitals could either lower the amount of administrated activity or shorten the acquisition times.

Method: Image acquisitions were performed with SPECT/CT using a NEMA-thorax phantom. The ratio between background and the hot spots, and the image statistics were calculated in clinical images to get realistic activity concentrations between background and hot-spots in the phantom. Images were reconstructed using the Evolution® algorithm altering the number of iterations. After acquisition with ^{99m}Tc, ^{123}I, ^{111}In and ^{177}Lu using ELEGP collimator and the clinically used collimator (LEHR and MEGP collimators) the image quality was evaluated with reference to SNR, contrast and noise.

Result: The ELEGP turned out to be the favourable collimator for ^{99m}Tc and ^{123}I in terms of SNR and noise levels compared to the LEHR collimator which is used in the clinical routine. The ELEGP collimator had less advantages compared to the MEGP collimator for ^{111}In and ^{177}Lu. A reason for the results for ^{111}In and ^{177}Lu could be due to Evolution Toolkit not supporting model based compensation for septum penetration and collimator scatter for the ELEGP collimator.

Conclusion: In this study, we demonstrated that ELEGP collimator is superior to the clinically used LEHR collimator for ^{123}I and we therefore propose that the ELEGP collimator is used in the clinic for examinations using ^{123}I. Examinations with ^{99m}Tc, ^{111}In and ^{177}Lu need to be further investigated.

Abbreviations

CBF	Cerebral Blood Flow
CDR	Collimator Detector Response
ELEGP	Extended Low Energy General Purpose
FWHM	Full Width at Half Maximum
^{123}I	Iodine-123
^{111}In	Indium-111
LEHR	Low Energy High Resolution
^{177}Lu	Lutetium-177
MEGP	Medium Energy General Purpose
MLEM	Maximum Likelihood Expectation Maximization
OSEM	Ordered-Subsets Expectation Maximization
PET	Positron Emission Tomography
PSF	Point Spread Function
ROI	Region Of Interest
RR	Resolution Recovery
SNR	Signal to Noise Ratio
SPECT	Single Photon Emission Computed Tomography
^{99m}Tc	Technetium-99m
TF	Transmitted Fraction

Table of content

Introduction

The use of radionuclides for diagnostic purposes has been around as far back as the middle of the twentieth century. Since then there has been many significant advances in nuclear medicine technology and it has become increasingly more common as a tool for diagnostic imaging [1]. An example of such an advance is the method of creating 3D images with single photon emission computed tomography (SPECT). Today over 10000 hospitals worldwide are using radionuclides to diagnose or treat patients. The use of nuclear medicine is still relatively small compared to the use of x-rays or magnetic resonance imaging (MRI) [2] but imaging using radiolabeled pharmaceuticals has some advantages over other modalities, such as being good at imaging physiology and metabolism.

To be able to visualise organ uptake or its functions, a radio-labelled pharmaceutical can be used, most imaging systems in nuclear medicine use collimators in front of the crystal. A relatively new parallel hole collimator; the extended low energy general purpose (ELEGP) has been created by GE Healthcare, which has larger holes compared to other low energy collimators. This will lead to the ELEGP collimator having higher sensitivity, but lower resolution. The ELEGP also has a thicker septum, which could give it the ability to image nuclides with higher energy without septum penetration.

The low resolution in the collimator means that the images created with the ELEGP collimator will have lower spatial resolution compared to images created with other low energy collimators. According to the manufacturer, GE Healthcare, the spatial resolution can be compensated for by using the modern reconstruction algorithm Resolution Recovery (RR) [3]. This has been shown for Octreoscan® with ^{111}In for liver tumours, which indicates that the ELEGP collimator could be a better choice of collimator [4].

If the ELEGP collimator could be proven to produce images with both lower noise levels and an acceptable spatial resolution and contrast, hospitals could either lower the amount of administrated activity or lower the acquisition times. Because of the long examination times with SPECT, lowering the acquisition time would be a great advantage. Another advantage would be if the ELEGP collimator could be used for the majority of examinations, so that collimator change between examinations would be unnecessary.

There have been relatively few studies done which evaluate the combination of ELEGP collimator and RR. At Umeå University there have been a couple of studies, where the image acquisition and reconstruction method are optimized for ^{111}In in small liver tumours. The consensus in these reports seem to be that the ELEGP collimator is the most optimal collimator for detecting small liver tumours with ^{111}In [4-7]. How the ELEGP collimator and ^{111}In performs with the SPECT/CT at Sahlgrenska University Hospital together with different radionuclides needs to be further investigated.

In this study the ELEGP was evaluated for four different patient examinations with four different isotopes; bone scintigraphy with ^{99m}Tc, Indium-111 (^{111}In)-penterotide-Octreoscan®, DaTSCAN™ with Iodine-123 (^{123}I) and investigation of the therapeutic effect of somatostatin positive tumours with Lutetium-177-[DOTA^{0},Tyr^{3}]- (^{177}Lu)-octreotate. These examinations were selected since they are frequently performed in the clinic and because the gamma energies are relevant for the ELEGP collimator.

To be able to fairly compare different collimators, the image acquisition must be optimized for the ELEGP collimator. The image acquisition for other collimators was assumed to be optimized. In this study the image acquisition was optimized with respect to the number of iterations.

Background

Nuclear medicine

In nuclear medicine a radioactive isotope is bound to a pharmaceutical and administrated to the patient either by injection, inhalation or oral administration. The radioactive isotope will be transported by the pharmaceutical to the site that is to be investigated.

Diagnostic images in nuclear medicine have some advantages over images from other modalities, such as being able to image compounds specific for a particular transport of pathway. Disadvantages are a relatively low spatial resolution and high noise levels.

In nuclear medicine different radiopharmaceuticals are used for specific biological processes, which can be divided into two subgroups; therapy and diagnostic imaging. In radionuclide therapy, the objective is to treat the patient either curative or palliative and the therapeutic response can, if the radionuclide emits photons, be evaluated using gamma cameras. In diagnosis, the objective is to detect photons emitted from the radiopharmaceutical and determine an activity distribution using external detectors. The diagnostic applications of nuclear medicine are more common than the therapeutic ones. In this study the focus will be on diagnostic applications.

In diagnostic nuclear medicine there are two main imaging modalities for detecting activity distributions; the gamma camera and positron emission tomography (PET). The gamma camera is using a collimator in front of the detector to be able to determine the activity distribution. In PET radio nuclides with positron emission is used and it uses the fact that annihilation photons spread with 180 degrees to each other to determine a distribution. In this study SPECT/CT will be used, which is an application of the gamma camera combined with a computed tomography (CT) scanner, where the camera rotates around the patient to create a tomographic image.

The gamma camera

The gamma camera, which is also called the Anger camera, was developed in late 1950's and the camera has primarily been used for diagnostic imaging [1]. The camera is able to determine activity distribution in the patient by detecting photons emitted by the administrated radiopharmaceutical. The gamma camera consists of a collimator, NaI(Tl)-crystal, light guide, a matrix of PM-tubes and electronics (Figure 1).

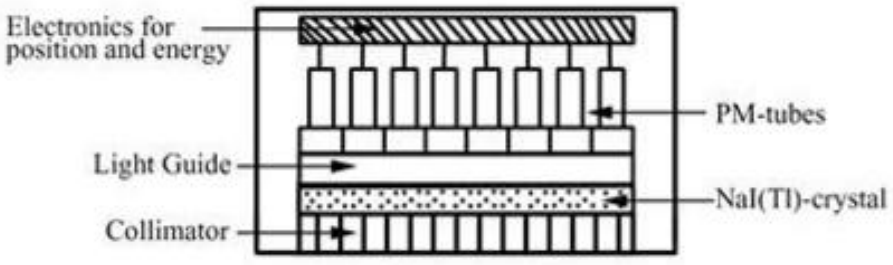

Figure 1: Schematic picture of the gamma camera.

The emitted photon will first reach the collimator, which is placed in front of the crystal. There are a few different types of collimators, for example the parallel hole collimator and the pinhole collimator.

The parallel hole collimator is by far the most common type of collimator and it consists of a lead plate with closely packed parallel holes. The holes are separated with a thin lead septum. To get as closely packed holes as possible, the holes are often hexagonal. The function of the collimator is to set an angle of detection, so that an activity distribution can be determined. If the holes are large and short, the collimator will accept a larger number of photons and the sensitivity will be high. The drawback of having large and short holes is that it is harder to determine which angle the photon came from and the spatial resolution will be low. The septum thickness will also influence the image. If the septum is to thin, the photon will penetrate the septum and a false signal will be detected. This can lead to star-shaped artefacts. If the the septum is too thick, the sensitivity will be low. When imaging nuclides with higher photon energies, a collimator with a thick septum is necessary to counteract septum penetration.

After the gamma photon has passed through the collimator, it hits the NaI(Tl)-crystal. The NaI(Tl)-crystal is a scintillation crystal where the gamma photon interacts and in turn produces light photons. The number of light photons created is proportional to the energy deposited in the crystal. If the crystal is thick, more gamma photons will interact in the crystal and the sensitivity will be high. The disadvantage of having a thick crystal is that it is harder to determine where in the crystal the energy is deposited and the spatial resolution will be low. Nowadays there are also gamma cameras that uses a semiconductor detector instead of a scintillation crystal. After the light photons are created in the crystal they will travel and reach the light guide, which will guide the light to a matrix of PM-tubes. In the PM-tubes the light will hit a photocathode, which converts the light into electrons. The numbers of electrons are then amplified by a chain of dynodes, and an electrical pulse can be measured. By knowing the size of the electrical pulse it is possible to calculate where the light photons originated. The electrical pulses are then processed in a matrix of electronics.

It can be shown both mathematically and experimentally that the sensitivity is independent of the distance between source and detector. It can also be shown that the spatial resolution depends strongly on the distance between source and detector.

It is important to avoid detecting too much scattered radiation. Since scattered gamma photons could have originated from anywhere in the patient, they will contribute to lower contrast. To avoid this, an energy window is placed around the photo peak that discriminates gamma energies that are outside the window. The window is typically around ±10% of the gamma energy. If the window is too narrow, the sensitivity will be low. If the window is too wide, the contrast will be low.

To obtain images with good noise levels, contrast and spatial resolution, the camera has to detect a sufficient amount of gamma photons. To save time, there are often two or three detectors that can detect at the same time mounted on the same gantry. The reason why even more detectors are not used is because the detectors need to come as close to the patient as possible. This is not possible with too many detectors. In SPECT the detectors are rotated around the patient with "step and shoot" technique. As the detectors rotate, projections from different angles are acquired. By using different reconstruction techniques a 3D-image can be created.

Radiopharmaceuticals

In nuclear medicine, the radiopharmaceutical is administrated to the patient by either injection, inhalation or by oral administration. The radiopharmaceutical consists of two components; a radioactive isotope and a pharmaceutical. The purpose of the pharmaceutical is to transport the radioactive isotope to different locations in the body. Where the radiopharmaceutical ends up depends on its physiological properties.

When selecting which radioactive isotope to use for diagnostics it is important to consider gamma energy, half-life, daughter nuclides or other types of the decay that contribute to the patient dose. If the gamma energy is too low, the attenuation will be high, which leads to too many gamma photons contributing to patient dose and not the image. If the energy is too high, the gamma photons will pass through the crystal and the sensitivity and spatial resolution will be low. Energies between 70 and 200 keV are most commonly used [7]. It is also important to consider physical and biological half-life. If the half-life is too short, the radiation will be gone before it can be injected and imaged or else a high activity amount needs to be injected to receive an image. If the half-life is too long and the activity is captured in the cell the patient dose can be too high. The by far most commonly used isotope is technetium-99m (^{99m}Tc), which has a half-life of 6 h. It is also important that the biological half-life of the radiopharmaceutical is long enough to be able to image the biological process.

^{99m}Tc

^{99m}Tc has a half-life of 6 hours and the gamma energy is 140 keV. The collimator used for ^{99m}Tc is usually a low energy high resolution (LEHR) or a low energy general purpose (LEGP). Bone scintigraphy is one of the most common examinations in nuclear medicine where ^{99m}Tc are bound to phosphate compounds that bind to bone. The amount of phosphate that binds to bone depends on blood flow and osteoblast production. Bone scintigraphy is used to diagnose bone metastases, osteitis and fractures. Patients at Sahlgrenska University Hospital are usually injected with 600 MBq of ^{99m}Tc-HDP/DPD three to four hours before a planar or/and SPECT/CT scan.

^{111}In

The half-life of ^{111}In is 2.8 days. The collimator used is a medium energy general purpose (MEGP), because of the high gamma energies at 171 and 245 keV. The diagnosis of tumours with somatostatin receptors is mainly performed with ^{111}In- Octreoscan® . ^{111}In is bound to a somatostatin analogue, penterotide, which binds to somatostatin receptors. Tumours with high concentrations of somatostatin receptors are usually tumours in the neuroendocrine system, examples are; carcinoids in small intestine, lung and pancreas. At Sahlgrenska University Hospital, SPECT/CT scan is done 24 hours after injection of 175 MBq ^{111}In -Octreoscan.

^{123}I

The gamma energy for ^{123}I is 159 keV, the half-life is 13.22 hours and the collimator used is the LEHR collimator. ^{123}I can be bound to DaTSCAN® which can be used to distinguish essential tremor from Parkinson-syndrome. In DaTSCAN® at Sahlgrenska University Hospital, 110-185 MBq ^{123}I is injected in the patient three hours before imaging. The ^{123}I binds to dopamine transporters in the basal ganglia which is visualised by a SPECT/CT scan.

^{177}Lu

^{177}Lu has a half-life of 6.7 days. It has two main gamma energies at 113 and 210 keV and a MEGP collimator is preferred. ^{177}Lu is a therapeutic nuclide when it is labelled to a somatostatin analogue, octreotate, which binds to somatostatin positive tumours. Since ^{177}Lu emits gamma photons it can be used to investigate the therapeutic effect of these somatostatin positive tumours and to find out the absorbed dose to healthy tissue. Examinations are done after every treatment cycle. At Sahlgrenska University Hospital, the patient is administrated with 7400 Mbq ^{177}Lu-octreotate with infusion for 30 minutes. Four planar scans within a week are performed as well as a SPECT/CT over the kidneys (dose limiting organ) the day after administration.

Iterative Reconstruction

In reconstruction for SPECT, raw data projections acquired in different angles of the patient are used to create a 3D-image of the activity distribution. There exist different kinds of methods and algorithms to reconstruct these projections. Because of the evolution of computing power, the dominating method today is iterative reconstruction methods, since it enables modeling of the detector systems. In this study, the iterative reconstruction maximum likelihood expectation maximization (MLEM) with ordered-subsets expectation maximization (OSEM) was used.

In all types of iterative reconstruction, the aim is to solve g=Af, where f is a vector of image data of a transversal slice, g is a vector of projection data from the same transversal slice and A is a matrix of probabilities that a gamma photon is detected such that g=Af. Direct inversion is often very slow and numerically unstable, the calculation are therefore done numerically. The ways the different methods differ are how the algorithms compare estimated projections and how they correct the estimation[8].

The basic concept for all iterative reconstruction methods is to numerically calculate a solution for projections from different angles. The reconstruction is initiated by first guessing a first estimate of f, often a uniform image. This image is then compared with the projections and then corrected. How the image is compared and corrected depends on the algorithm.

MLEM uses the following algorithm:

$$\bar{f}_j^{\,k+1} = \frac{\bar{f}_j^{\,k}}{\sum_{i=1}^{n} a_{ij}} \sum_{i=1}^{n} \frac{g_i}{\sum_{j=1}^{m} a_{ij} \bar{f}_j^{\,k}} a_{ij},$$

where $\bar{f}_j^{\,k+1}$ is the new image data, $\bar{f}_j^{\,k}$ is the old image data, a_{ij} is the probability that a gamma photon from pixel j is detected at bin i and g_i is the projection data. The MLEM-algorithm works by finding a solution estimate for f by maximizing the likelihood for the mean number of counts $\bar{f}$ in an image to produce g. This is done by using the Poisson law[9]. The MLEM algorithm takes a long time for computers to calculate. To solve this problem, OSEM is used. OSEM groups projections evenly distributed around the patient into subsets. OSEM then sums the counts of the projection in each subset and reconstructs an image by using MLEM. The decrease in computing time is approximately equal to a factor of the number of subsets used[7].

Corrections

Attenuation

When imaging a patient, the goal is to find the distribution of activity. A problem is that gamma photons have a varying probability of being attenuated before reaching the detector depending on where the emission originated in the patient. Without any corrections for this effect, images will underestimate the amount of activity deep in the patient and behind materials with a high electron density, such as bone. To be able to perform corrections for attenuation, a patient-specific attenuation map is needed [9]. An excellent way to make an attenuation map, is by using CT-images, where the amount of HU in a voxel represents the electron density. The easiest way to obtain well registered CT-images is by using SPECT/CT, where the gamma camera detectors are mounted on a CT gantry. A drawback by using CT is the extra dose to the patient.

An advantage of using MLEM is that it is relatively easy to correct for attenuation by adding corrections into the matrix of probabilities A (see Iterative Reconstruction). The attenuation is first calculated for every voxel and the transmitted fraction (TF) is then included into the probability matrix. To calculate the attenuation from position (t′, s) the following formula is used:

$$TF = \exp\left(-\int_{s'}^{\infty} \mu(t', s)ds\right),$$

where $\mu(t', s)$ is the linear attenuation coefficient as a function of position [9].

Scatter

Gamma photons registered in the crystal are not only primary gamma photons but scattered gamma photons as well. The problem with detecting scattered gamma photons is that they hold false information about where the original emission happened and will cause the image contrast to be worse. There are a few ways to correct for this. The method which is most commonly used, is where an energy window is placed over the photopeak of the transmitted gamma energy to discriminate all other energies. Another method is where an additional energy window is placed in the Compton area and then is subtracted from the image.

Collimator detector response (CDR)

CDR describes loss in spatial resolution, which is responsible for blurring in images. The spatial resolution for the imaging system is described by the point spread function (PSF) [5]. The source of blurring consists of four main sources; the intrinsic resolution of the system, the geometrical acceptance of photons through the collimator, septum penetration and septum scatter [3]. The intrinsic resolution depends on the uncertainty in determining where the photon interaction happened in the crystal. There is also an uncertainty in the electronics. Intrinsic resolution is independent of source to detector distance and can be modeled by a Gaussian function.

The geometrical acceptance of photons through the collimator depends on the source to detector distance due to the holes accepting photons from a larger area at larger distances. The blurring due to this effect depends strongly on the source to detector distance. The blurring can be modeled by a Gaussian function, where the standard deviation is a linear function of distance. The standard deviation of the PSF for both effects can be described by the following formula:

$$\sigma_C = \sigma_0 + \sigma_d * d,$$

where σ_C is the standard deviation of the PSF approximated with a Gaussian function, σ_0 is the standard deviation at the collimator, σ_d is the change of standard deviation with distance and d is the distance from the collimator [9]. By knowing the source to detector distance and approximating the PSF with a Gaussian function, it is possible to correct for loss in spatial resolution by implementing the model into the probability matrix (see Iterative Reconstruction) when performing iterative reconstruction [7]. When using this correction, it could be possible that the use of collimators that accept a higher number of photons is more optimal for better image quality. A drawback to performing this correction is that it is time consuming for computers to calculate. Another faster method for correcting blurring effects is by adding a filter after the reconstruction is finished. This method was not investigated in this study. Septum penetration and septum scatter corrections are only included in the CDR compensation for the MEGP collimator in this study.

The gamma photons emitted from the patient always have a chance of passing through the septum of the collimator. This will decrease the image contrast and may also lead to star shaped artefacts. One way to counteract this problem is to increase the septum thickness but this will also have negative impact on the efficiency. There are some other methods to deal with septum penetration and septum scatter. Energy window discrimination can exclude a large portion of the scattered photons, but there will still be a problem with the penetrating non-scattered gamma photons within the energy window.

Septum penetration is modelled when reconstructing raw data acquired with the MEGP collimator and included in the CDR compensation but not yet implemented for the ELEGP collimator.

Material and Method

Phantom preparation

In the evaluation of ELEGP collimator for SPECT/CT with different radionuclides, a Body Phantom Set™ designed and modified by International Electrotechnical Comission (IEC) and National Electric manufacturers Association (NEMA), respectively (NEMA IEC body Phantom Set™, Model PET/IEC-BODY/P-2007-Data Spectrum, Durham, USA) was used (Figure 2). The NEMA phantom will mimic a thorax of a patient with tumors of varying sizes. The NEMA phantom was used for evaluation of the image quality with ^{99m}Tc, ^{111}In, ^{123}I and ^{177}Lu. The phantom was filled with water to approximate body tissue. The dimensions of the spheres (hot-spots) in the NEMA phantom are shown in Table 1. The length of the NEMA phantom is 180 mm and volume is 9.7 litres.

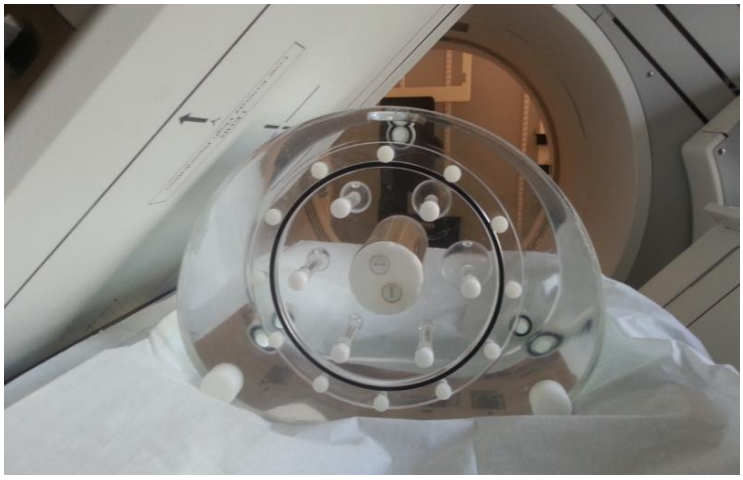

Figure 2: NEMA thorax phantom placed in gamma camera.

Table 1: Sphere dimensions for the NEMA phantom according to the manufacture, where sphere 1 is the largest sphere and sphere 6 is the smallest sphere.

Sphere	Sphere Diameter (mm)	Sphere Volume (mL)
1	37	26.52
2	28	11.49
3	22	5.57
4	17	2.57
5	13	1.15
6	10	0.52

The activity distribution in the phantom was estimated by analysing clinical SPECT projection images. Five patients from each examination were chosen randomly. The examinations that were analysed to get similar statistics in the phantom images versus images acquired in clinical settings were bone scintigraphy for ^{99m}Tc, ^{123}I-DaTSCAN™ (ioflupane ^{123}I-injection), ^{111}In-Octreoscan® and ^{177}Lu-octreotate. The background activity distribution was analysed by placing a region of interest (ROI) close to the hot-spots in the clinical image and measuring the mean pixel value. Hot-spots were analysed by drawing a ROI over the hot-spot in the image and measuring the maximum pixel count. This is a well established procedure to avoid underestimation of the uptake due to partial volume effects. Thereafter counts per unit length were calculated for every area, which corresponds to the

relative uptake. All hot-spot to background ratios were calculated by taking the mean from five patients. In planar images there are no attenuation corrections. This was accounted for by measuring the depth of the different areas and correct for attenuation by approximating the patient density with water.

To know the amount of activity that the background of the NEMA phantom was to be filled with, the initial injected activity was divided by 60 kg (a small patient) and then multiplied by 9.7 kg (weight of phantom). A relatively light patient weight was chosen not to underestimate the activity injected in the phantom. The activity was multiplied by two to be able to decrease the acquisition time. To know the activity to the spheres, the background activity was multiplied with the ratio acquired in the patient images.

The activity concentrations used for the background and spheres (i.e. hot-spots) were calculated and corrected for decay for each radionuclide. The activity (±10 % of the calculated activity) was transferred from the vial to the water-filled background of the phantom using a syringe. The activity in the syringe was measured before and after administration into the phantom to be able to know the obtained activity concentration. To achieve a homogenous activity distribution in the background, a small air bubble was left in the background and the phantom was rolled around. After blending the activity, the phantom was filled completely.

To fill the spheres, the activity was transferred with a syringe to a bottle filled with a known amount of water. The syringe was measured before and after administration into the bottle, and the activity concentration was calculated, all spheres were filled with the same activity concentration.

SPECT imaging

The gamma camera used for all image acquisitions in this study was a SPECT/CT with a diagnostic CT (Discovery NM/CT 670, GE Healthcare, Waukesha, WI) (Figure 3). The workstation platform used was Xeleris 3.1067 (GE Healthcare). All reconstruction were made using Evolution® algorithm [3].

Figure 3: Discovery NM/CT 670 used for all image acquisitions.

The collimators used in this study were the ELEGP, LEHR and the MEGP collimators from GE Healthcare. The dimensions of these collimators can be seen in Table 2.

Table 2: The dimensions for the collimators from GE used in this study.

Collimator	Hole diameter (mm)	Hole length (mm)	Septal thickness (mm)
ELEGP	2.5	40	0.4
LEHR	1.5	35	0.2
MEGP	3	58	1.05

After the phantom was filled, it was placed on its "back" in the gamma camera with the largest sphere to the left (seen from gantry, Figure 2). The acquisition time was calculated to receive image statistics comparable to the statistics in patient images by performing a short test scan. A ratio between mean count from the background in the short test scan and the mean count in high uptake background in patient images was calculated. The ratio was multiplied with the acquisition time for the short test scan, to get the acquisition time needed in order to get similar image statistics in the phantom images and clinical images, and the acquisition time also had to be corrected for decay for every scan. All images were done with 120 projections.

For every type of examination two collimators were used; the collimator chosen traditionally in the clinic and the ELEGP collimator. For ^{99m}Tc and ^{123}I, and for ^{111}In and ^{177}Lu the LEHR and MEGP collimators were used respectively. After every SPECT scan a CT scan was performed to be able to correct for attenuation. The acquisition was performed four times for every collimator for all examinations to be able to see statistical variations.

Reconstruction

All images were reconstructed using a reconstruction software program Evolution toolkit® (GE Healthcare, Evolution for bone with Volumetrix MI in Xeleris). This is a model-based corrective SPECT image reconstruction method which compensates for resolution degradation caused by CDR [3]. To test the optimal number of iterations for ELEGP, one through five OSEM iterations with ten subsets were performed for all four ELEGP images for every nuclide in this study. Images acquired with other collimators were also reconstructed with one through five OSEM iterations with ten subsets.

CT-based attenuation corrections were performed and correction for CDR. CDR included model based corrections for septum penetration and collimator scatter for the MEGP collimator but not for the LEHR and ELEGP collimators. No filtering was used.

Image quality

Analysis of regions of interest

All reconstructed images were analysed one at a time choosing the slice where the hot-spots were the largest. A number of ROIs were positioned over the background at a distance from any hot-spots and edges. An average pixel count and standard deviation were noted. The hot-spots were analysed by

defining a ROI with a radius to full width half maximum (FWHM), Figure 4, and an average pixel count was obtained. All hot-spots that were visible at FWHM were analysed.

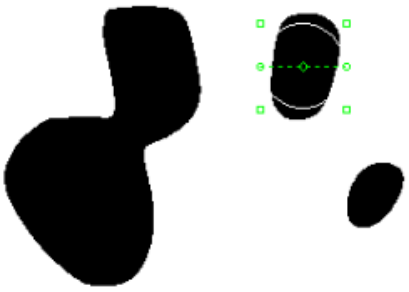

Figure 4: ROI defined over the third largest sphere in the NEMA phantom with Xeleris. The windowing was set at 50% of the maximum count in the sphere and the ROI is placed at FWHM. The slice used is where the spheres are the largest.

To know the optimal number of OSEM iterations for ELEGP collimator for every nuclide, the signal to noise ratio (SNR) was plotted as a function of number of OSEM iterations with 10 subsets for every sphere. SNR was calculated in the following way:

$$SNR = \frac{|\bar{s} - \bar{b}|}{\bar{\sigma}_b},$$

where $\bar{s}$ is the mean signal count measured at FWHM for a sphere, $\bar{b}$ is the mean background count measured from twelve ROIs with 90 voxels each placed in the background and $\bar{\sigma}_b$ is the mean of the standard deviation of the number of counts per pixel in the same twelve background ROIs.

To evaluate the image quality in the reconstructed images, contrast was plotted against noise obtained from the images reconstructed with one through five iterations. The contrast in the spheres was calculated in the following way:

$$C = \frac{\bar{s} - \bar{b}}{\bar{b}},$$

and the image noise was calculated from:

$$N = \frac{\bar{\sigma}_b}{\bar{b}}.$$

Evaluation by adding noise

A reduction in acquisition time using ELEGP collimator was investigated by adding Poisson noise to the ELEGP raw data images until the SNR or noise levels matched the images acquired with the

traditionally used collimator. This was only done with images acquired with ^{123}I, because this was the only nuclide where the ELEGP collimator produced images with higher SNR for clinically relevant sized spheres.

Analysis of profiles

In order to investigate the spatial resolution and Gibbs artefact, a profile was placed in the ^{123}I-images acquired with both collimators. The profile was placed over sphere 1 and sphere 4 (Figure 5). The FWHM was then measured for both spheres.

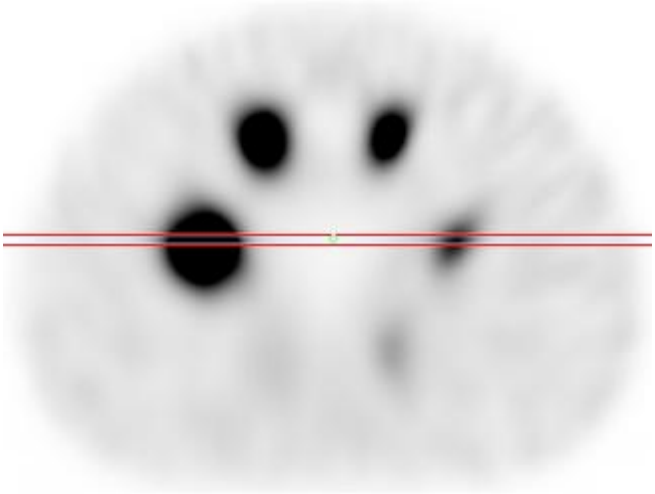

Figure 5: Profile placed over sphere 1 and 4 in the NEMA phantom.

Statistical analysis

To get some statistics to work with and to reduce the uncertainties, four image acquisitions were done for every collimator and examination. All results in this study were expressed as standard error of the mean, calculated in the following way:

Standard deviation: $\sigma = \sqrt{\frac{1}{n-1}\sum_{i=1}^{n}(x_i - \bar{x})^2}$

Error propagation: $s = \sqrt{\left(\frac{\partial f}{\partial x}\right)^2 s_x^2 + \left(\frac{\partial f}{\partial y}\right)^2 s_y^2 + \left(\frac{\partial f}{\partial z}\right)^2 s_z^2 + \cdots}$

Standard error of the mean (SEM): $SEM = \frac{s}{\sqrt{n}}$,

where n is the number of acquisitions, x_i is the measurement, $\bar{x}$ is the mean of the measurements and S_f represents the standard deviation of the function f.

Results

In this study, four different SPECT/CT examinations (with four different radionuclides i.e. ^{99m}Tc, ^{123}I, ^{111}In and ^{177}Lu) were tested to find out which collimator that is most suitable for respective radionuclide. The evaluation of ELEGP collimator was compared to the evaluation of the traditionally used LEHR or MEGP collimator.

The optimal number of iterations after acquisition using the ELEGP collimator was investigated for every nuclide. SNR was plotted as a function of the number of OSEM iterations with ten subsets and different spheres in the NEMA phantom were compared. Images acquired using the two collimators for every nuclide were compared by plotting the contrast as a function of noise for one through five OSEM iterations for both collimators for every sphere separately.

SPECT/CT evaluation of an ELEGP collimator versus a LEHR collimator for ^{99m}Tc

The images after SPECT/CT acquisition with ^{99m}Tc for bone scintigraphy were evaluated to find the optimal number of iterations used for the ELEGP collimator. SNR was plotted as a function of OSEM iterations with ten subsets for the three largest spheres, Figure 6. The spheres were filled with an activity concentration which was 6.1 times higher than the background concentration. The optimization plot shows that larger spheres had the highest SNR when two OSEM iterations were performed. The difference in SNR was smaller for smaller spheres and the SNR declinened after two iterations. Only three out of six spheres were analysed because the FWHM of the signal for the smallest spheres drowned in background counts. In Figure 6, error bars display SEM from four image acquisitions.

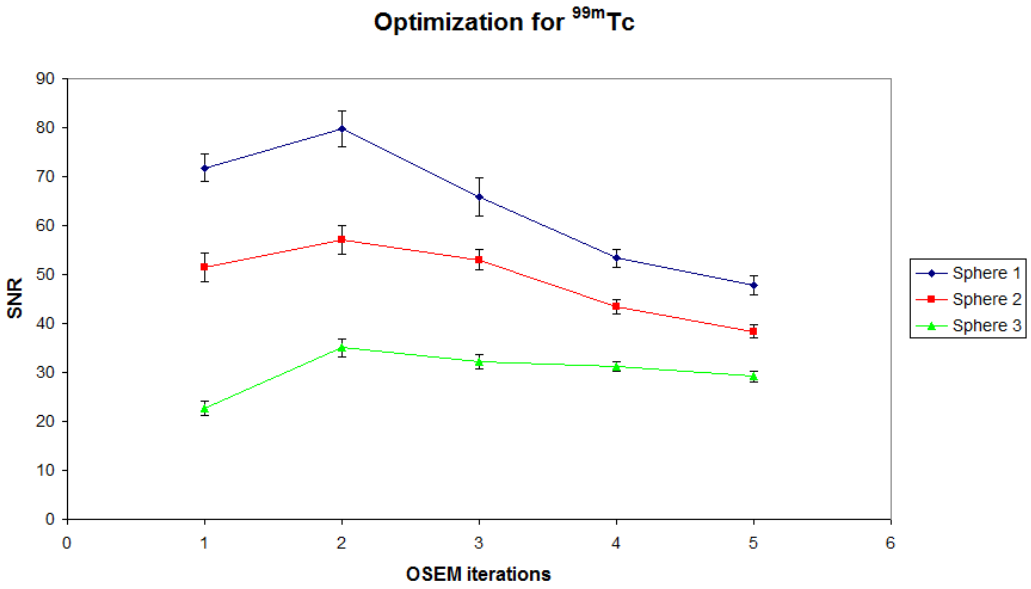

Figure 6: SNR plotted as a function of OSEM iterations with ten subsets for the NEMA-phantom with ^{99m}Tc applied on a bone scintigraphy protocol using the ELEGP collimator. Sphere 1 is the largest sphere and Sphere 3 is the third largest sphere. Error bars indicate SEM.

For the evaluation of contrast and noise levels between ELEGP and LEHR collimator, the contrast as a function of noise was plotted for sphere 1 to 3 with one to five OSEM iterations (Figures 7 and 8).

The contrast for both collimators leveled out relatively early for spheres 1 and 2. If the iterations were compared separately, the noise levels were lower for the ELEGP collimator. The difference in contrast level decreased with the size of the spheres.

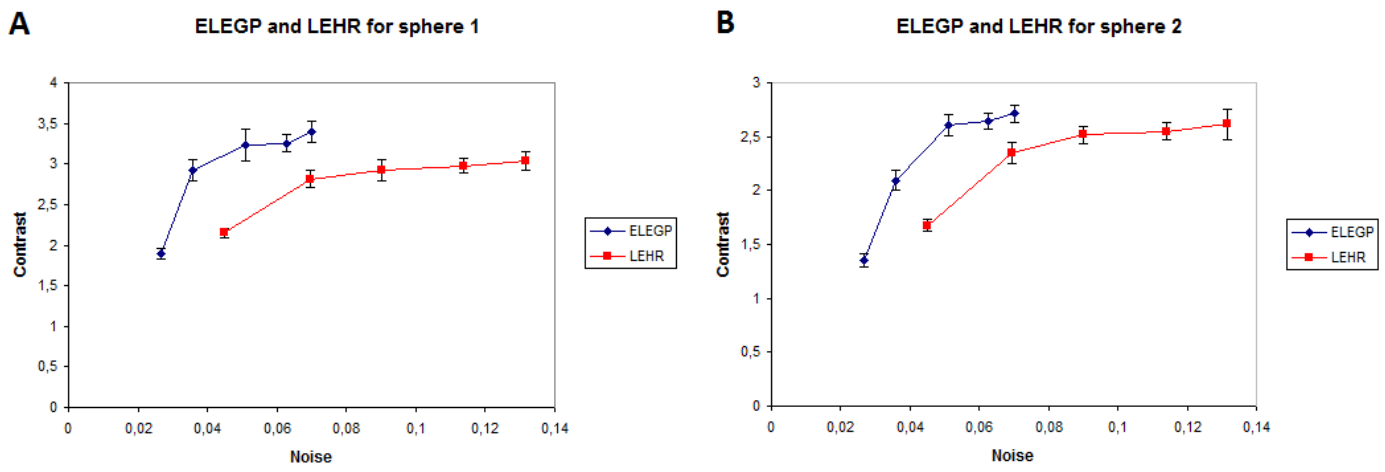

Figure 7: Contrast plotted as a function of noise for both ELEGP and LEHR collimators for ^{99m}Tc with a bone scintigraphy protocol for A: sphere 1 and B: sphere 2. Five noise levels were generated with one (lowest noise level) to five (highest noise level) OSEM iterations with ten subsets. The noise increased with the number of OSEM iterations for both collimators. Error bars indicate SEM.

Because sphere 3 is the smallest sphere that could be analysed and it has most similar size to the smallest bone tumours that can be detected in the clinical situation, the sphere 3 images were further investigated. The contrast to noise graph was plotted separately (Figure 8). The SNR value was 35.0 and 32.3 for two and three iteration steps, respectively, for the ELEGP collimator and 25.4 for the LEHR collimator with two iterations. These SNR values are displayed because they are the highest SNR values for each collimator. The difference in contrast was smaller than for sphere 1 and 2. Higher number of iterations gave higher noise levels. LEHR collimator has a higher noise level than the ELEGP collimator for the same number of iterations.

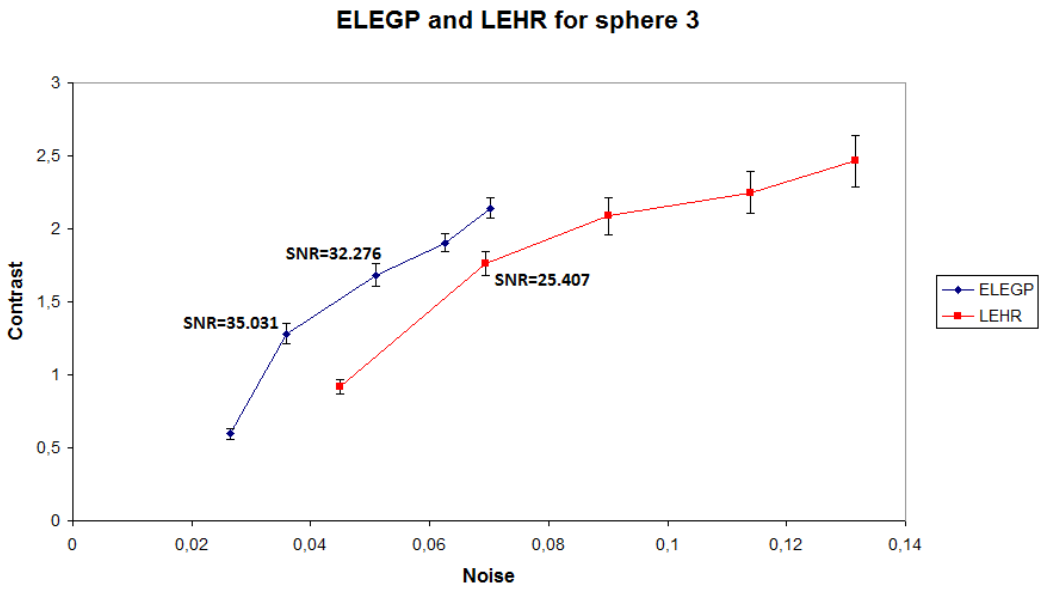

Figure 8: Contrast plotted as a function of noise for both ELEGP and LEHR collimators for ^{99m}Tc with a bone scintigraphy protocol for sphere 3. The five noise levels are generated with one (lowest noise level) to five (highest noise level) OSEM iterations with ten subsets. The noise increased with the number of OSEM iterations for both collimators. SNR is displayed for the most relevant iteration steps. Error bars indicate SEM.

The images with the highest SNR for both collimators for ^{99m}Tc applied on a bone scintigraphy protocol can be seen in Figure 9. A higher number of iterations resulted in a noisy image. When using LEHR collimator, the image is noisier than for images with the ELEGP collimator. Ideally, sphere 4 would have been analysed instead of sphere 3, but this could not be done due to the FWHM of sphere 4 drowning in the high background count.

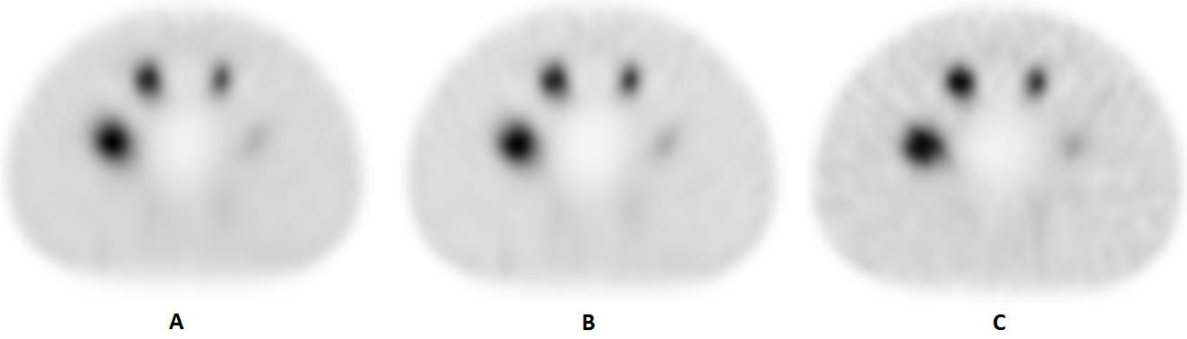

Figure 9: Images of the phantom using a protocol for bone scintigraphy. A: Two iterations with ELEGP. B:Three iterations with ELEGP. C: Two iterations with LEHR (used clinically).

SPECT/CT evaluation of an ELEGP collimator versus a MEGP collimator for ^{111}In

In Figure 10 the optimization for ^{111}In-penterotide is shown for the four largest spheres. Data from one and two iterations for sphere 4 could not be obtained due to the sphere signal drowning in the high background signal. The spheres were filled with an activity concentration which was 15.7 times higher than the background concentration. SNR was much lower for smaller spheres and the number of iterations mattered less for small spheres. For spheres 3 and 4 it is even possible that three or more iterations were optimal.

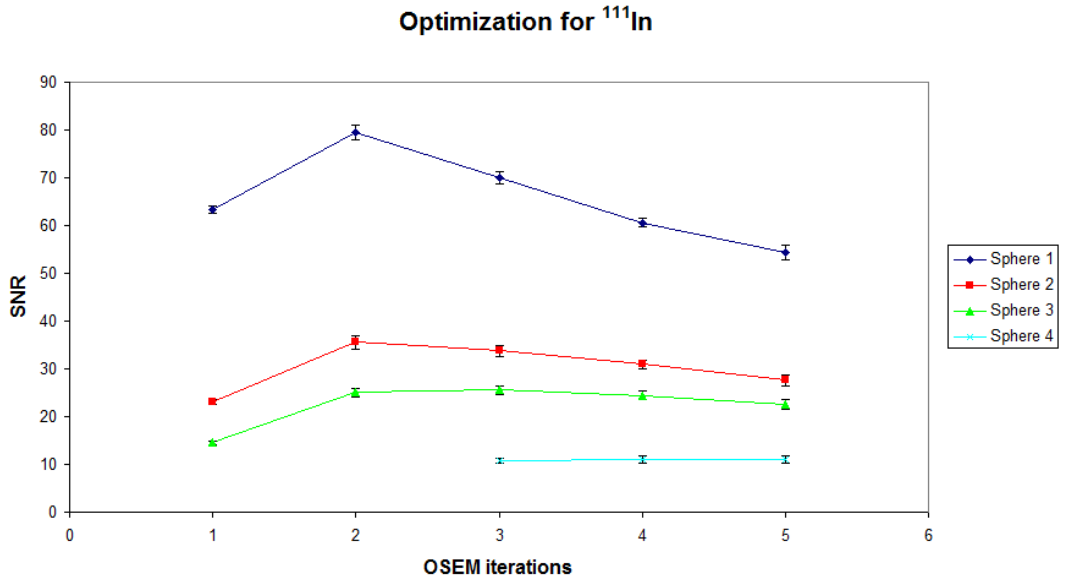

Figure 10: SNR plotted as a function of OSEM iterations with ten subsets for the NEMA-phantom with ^{111}In applied on an Octreoscan protocol using the ELEGP collimator. Sphere 1 is the largest sphere and Sphere 4 is the fourth largest sphere. The error bars indicate SEM.

To compare ELEGP to MEGP collimator for ^{111}In, the contrast was plotted as function of noise in Figure 11. The plot for the largest sphere shows that the images with MEGP collimator had higher contrast than the images using ELEGP collimator. If the second iteration was compared between collimators, the noise level and SNR was lower for the ELEGP collimator than for the MEGP collimator. The contrast curves for the ELEGP collimator and the MEGP collimator were closer to each other for sphere 2 compared to sphere 1 but the MEGP was still superior.

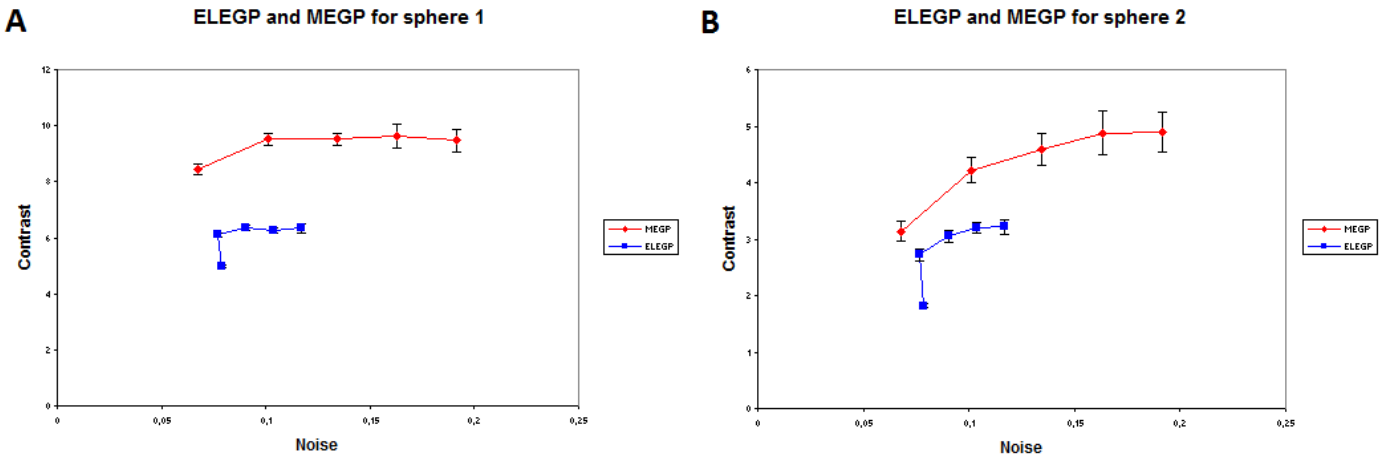

Figure 11: Contrast plotted as a function of noise for one to five OSEM iterations with ten subsets, for A: sphere 1 and B: sphere 2. The collimators shown are both ELEGP an MEGP and the nuclide used is ^{111}In. The five noise levels were generated with one to five OSEM iterations with ten subsets. The lowest noise level for the ELEGP collimator was generated with two OSEM iterations. The second lowest noise level with the ELEGP collimator was generated with one OSEM iteration and the noise then increased with an increased number of itarations up to five OSEM

iterations. For the MEGP collimator, the noise increased with an increased number of iterations. The error bars indicate SEM.

The most relevant spheres were sphere 3 and 4 because of their similar size to the smallest tumours that can be detected. The contrast to noise graphs for these spheres are shown in Figure 12. The MEGP collimator was superior to the ELEGP collimator for sphere 3. The graphs also show that the curves flatten out slower for smaller spheres which indicates that small spheres were more effected by low spatial resolution. Two iterations for images taken with MEGP collimator still had a higher SNR than images using ELEGP collimator for sphere 4.

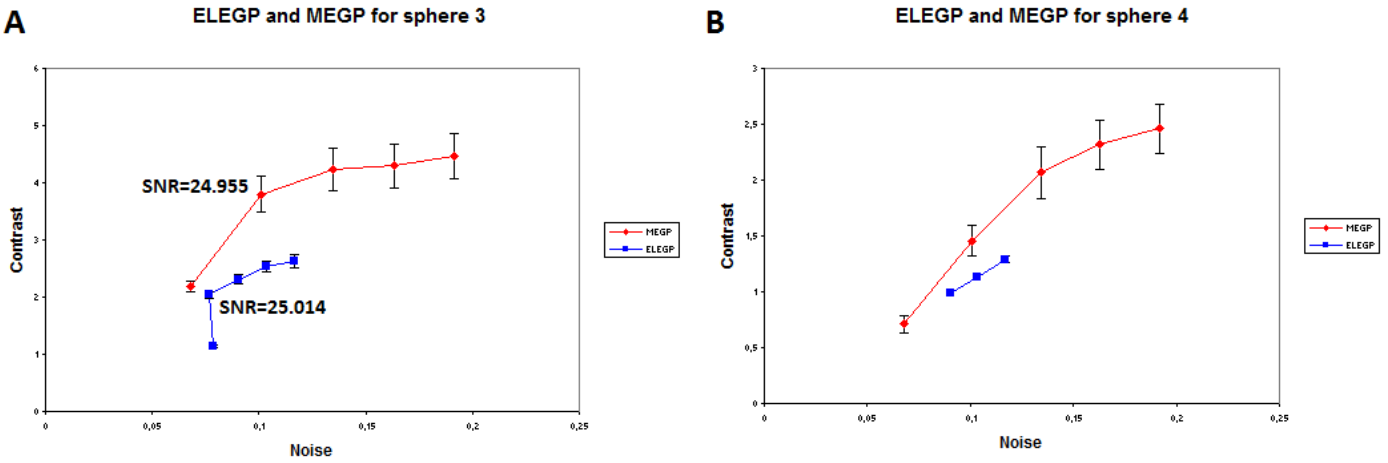

Figure 12: Contrast plotted as a function of noise for one to five OSEM iterations for A: sphere 3 and B: sphere 4 where iterations one and two for the ELEGP collimator could not be displayed. The collimators shown are both ELEGP and MEGP collimators and the nuclide used was ^{111}In. The five noise levels were generated with one to five OSEM iterations with ten subsets. The lowest noise level for the ELEGP collimator was generated with two OSEM iterations. The second lowest noise level with the ELEGP collimator was generated with one OSEM iteration and the noise then increased with an increased number of itarations up to five OSEM iterations. For the MEGP collimator, the noise increased with an increased number of iterations. The error bars indicate SEM. The SNR is displayed for the most relevant iteration steps.

The images with the highest SNR for each collimator are displayed in Figure 13, the image where the MEGP collimator was used has higher contrast.

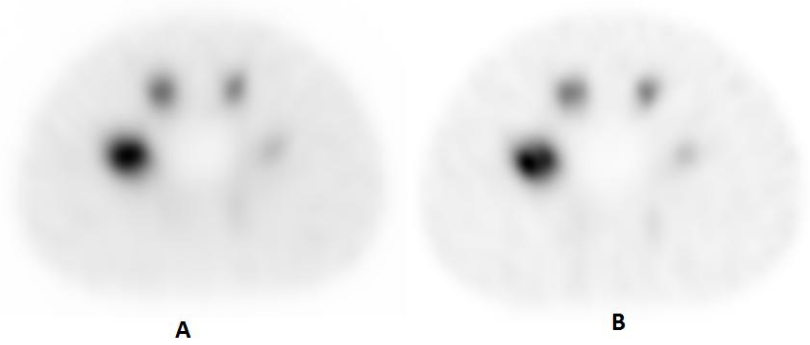

Figure 13: Images of the NEMA phantom with the highest SNR for both collimators using a protocol for ^{111}In-octreoscan. A: Two OSEM iterations and ten subsets with the ELEGP collimator. B: Two OSEM iterations and ten subsets with the MEGP collimator (used clinically).

SPECT/CT evaluation of an ELEGP collimator versus a LEHR collimator for ^{123}I

The optimal number of OSEM iterations was found by plotting SNR as a function of the number of OSEM iterations for the four largest spheres after acqusition with ^{123}I, Figure 14. The spheres in the NEMA phantom were filled with an activity concentration 18.7 times higher than the background concentration. The SNR was highest at one iteration for sphere 1. For sphere 2 and 3, two iterations gave the highest SNR. Two through five iterations gave approximately the same SNR for sphere 4.

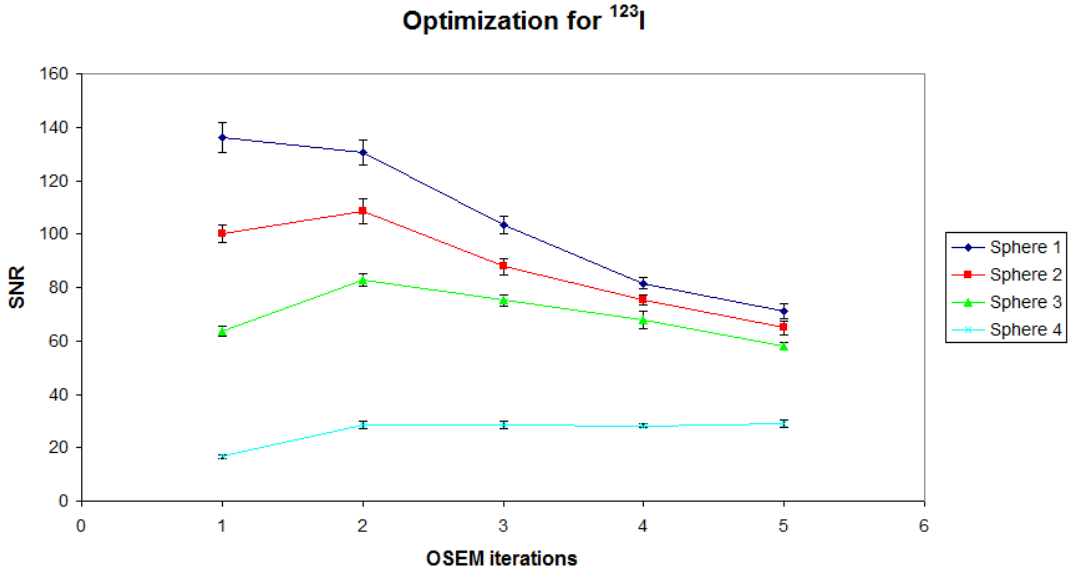

Figure 14: SNR plotted as a function of OSEM iterations with ten subsets for the NEMA-phantom with ^{123}I using a DaTSCAN™ protocol and the ELEGP collimator. Sphere 1 is the largest sphere and Sphere 3 is the fourth largest sphere. The error bars display SEM.

To evaluate and compare the performance of the ELEGP collimator, contrast was plotted as a function of noise generated from five OSEM iteration steps with ten subsets. The graphs for the two largest spheres can be seen in Figure 15, where the ELEGP collimator is compared to the LEHR collimator for ^{123}I. Figure 14 shows that the contrast was higher for the ELEGP collimator compared to the LEHR collimator for these spheres.

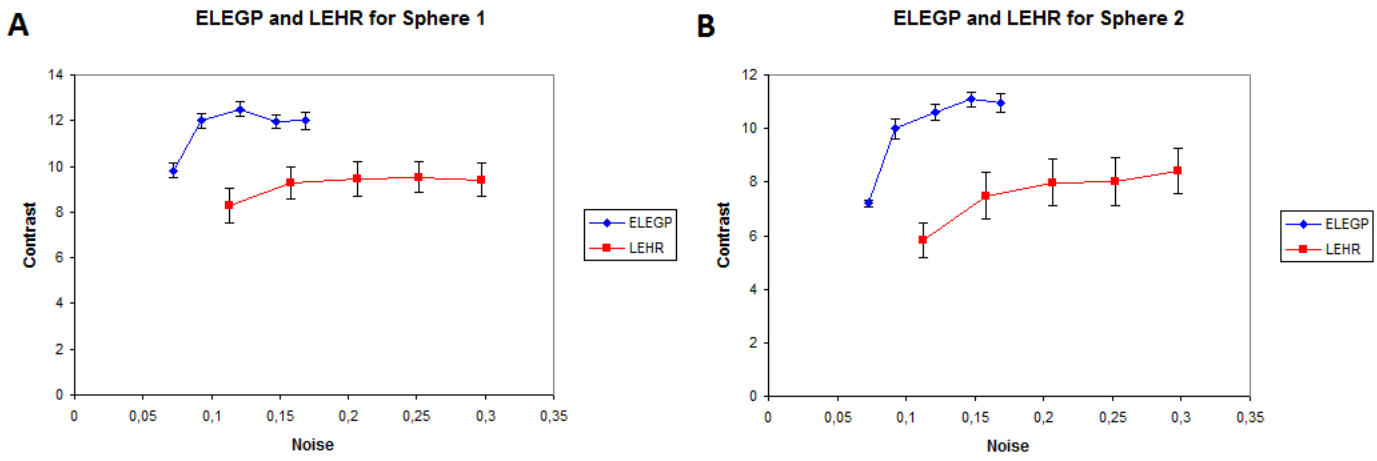

Figure 15: Contrast plotted as a function of noise for one to five OSEM iterations for A: sphere 1 and B: sphere 2. The collimators shown are both ELEGP and LEHR and the nuclide used is ^{123}I. The five noise levels were generated with one (lowest noise level) to five (highest noise level) OSEM iterations with ten subsets. The noise increased with the number of OSEM iterations for both collimators. The error bars display SEM.

The results for sphere 3 and 4 can be seen in Figure 16. The graphs compare contrast and noise for the ELEGP and LEHR collimators. The difference in contrast between the collimators was smaller for sphere 4 but for the ELEGP collimator the contrast-to-noise ratio was superior. Artificial Poisson noise was added to the second iteration for the ELEGP collimator until the SNR matched the SNR for the second iteration for the LEHR collimator. This was done for the most relevant sphere; sphere 4. The results showed that Poisson noise which corresponded to 50% of the total acquisition time had to be added to the image before SNR matched in images using the LEHR collimator matched. This indicate that the acqusition time can be reduced if the ELEGP collimators is used instead of LEHR collimator.

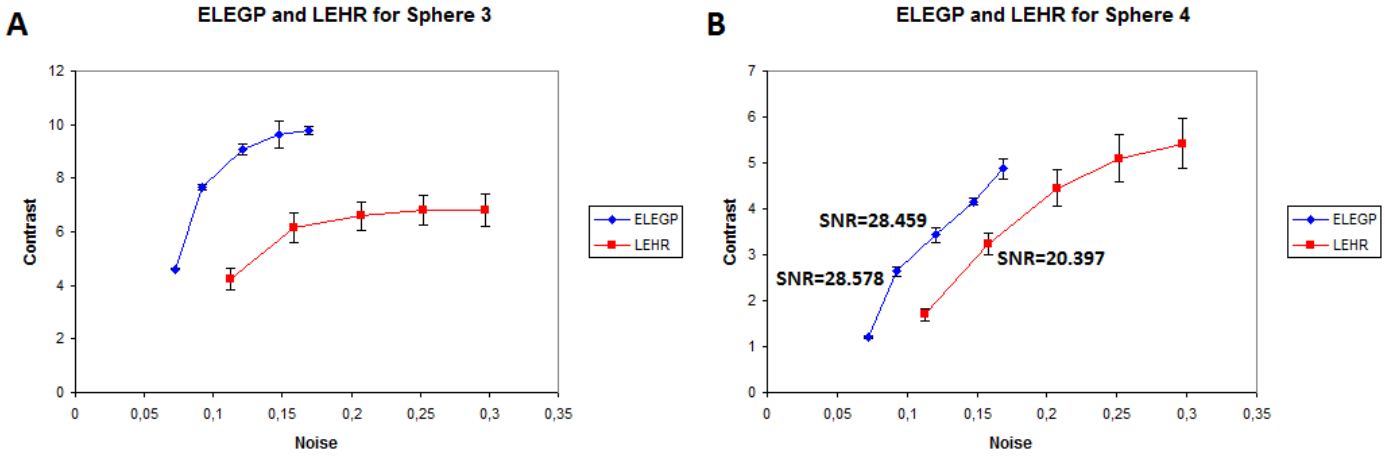

Figure 16: Contrast plotted as a function of noise for one to five OSEM iterations for A: sphere 3 and B: sphere 4. The collimators shown are both ELEGP and LEHR and the nuclide used is ^{123}I. The five noise levels were generated with one (lowest noise level) to five (highest noise level) OSEM iterations with ten subsets. The noise increased with the number of OSEM iterations for both collimators. The error bars displays SEM. The SNR is displayed for the most relevant iteration steps.

The images with the highest SNR for both collimators are displayed in Figure 17. The image where the LEHR collimator was used gave a noisier image compared with images using the ELEGP collimator.

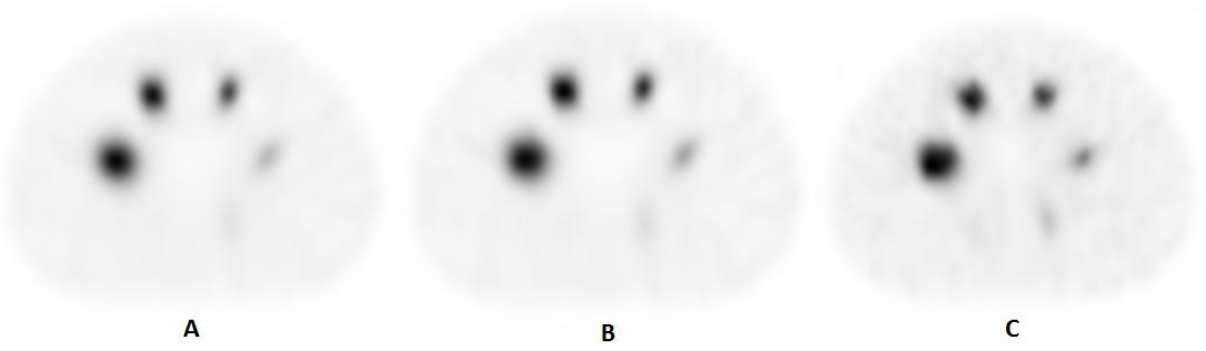

Figure 17: Images of the NEMA phantom with the highest SNR for both collimators using a protocol for ^{123}I-DaTSCAN™. A: Two OSEM iterations and ten subsets with the ELEGP collimator. B: Three OSEM iterations and ten subsets with the ELEGP collimator. C: Two OSEM iterations and ten subsets with the LEHR collimator (used clinically).

To analyse the spatial resolution and Gibbs artefact, a profile was placed over sphere 1 and 4 in the NEMA phantom. The profiles are displayed in Figure 18. The LEHR collimator gave higher resolution than the ELEGP collimator for sphere 4, but it also gave lower resolution for sphere 1. Gibbs artefact could not be identified in any of the profiles.

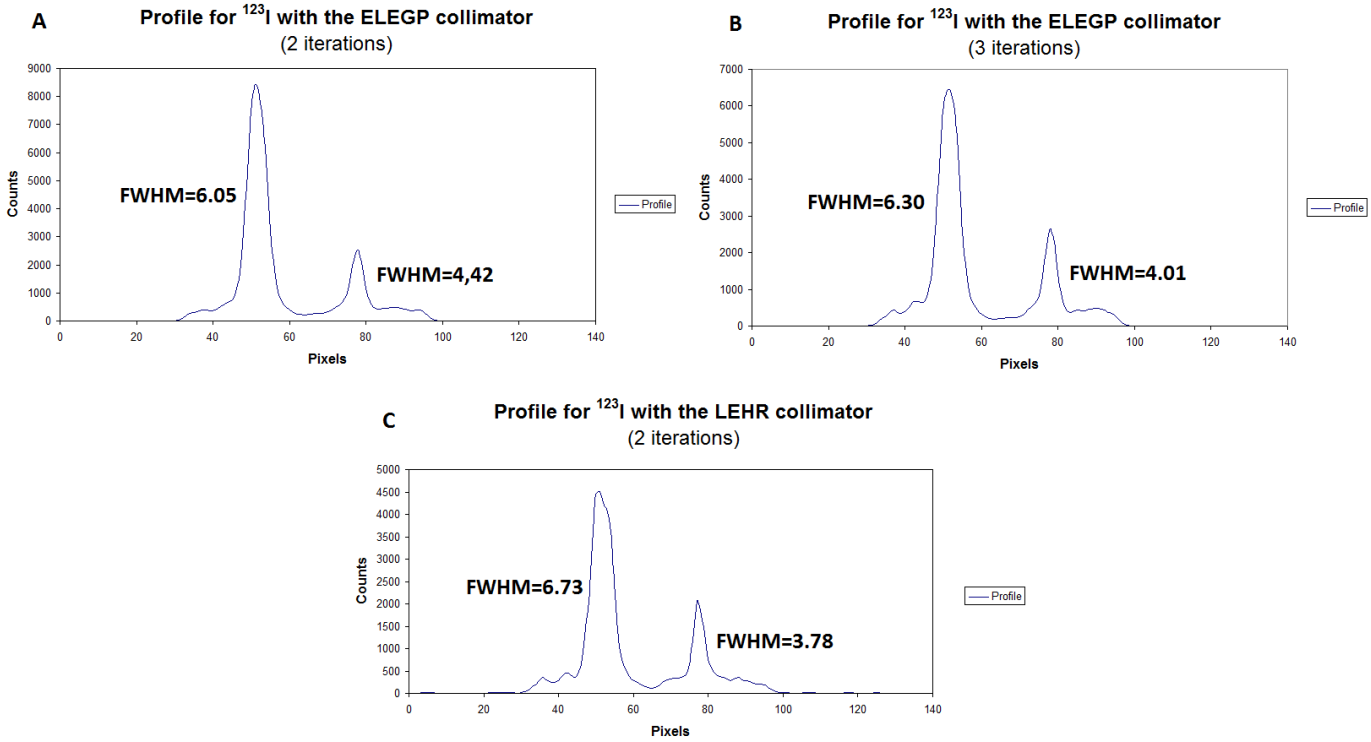

Figure 18: Profiles placed over sphere 1 (left peak) and 4 (right peak) in the NEMA phantom with images acquired with A: two iterations with the ELEGP collimator. B: Three iterations with the ELEGP collimator. C: two iterations with the LEHR collimator. The FWHM is displayed for each sphere.

SPECT/CT evaluation of an ELEGP collimator versus a MEGP collimator for ^{177}Lu

In Figure 19, SNR is plotted as a function of number of OSEM iterations to find the optimal number of OSEM iterations for the ELEGP collimator. The four largest spheres in the NEMA phantom are shown. The spheres were filled with an activity concentration which was 14.5 times higher than the background concentration. Reconstructions with two iterations had the highest SNR for all spheres, except for sphere 4, where iteration steps 3, 4 and 5 had the highest SNR.

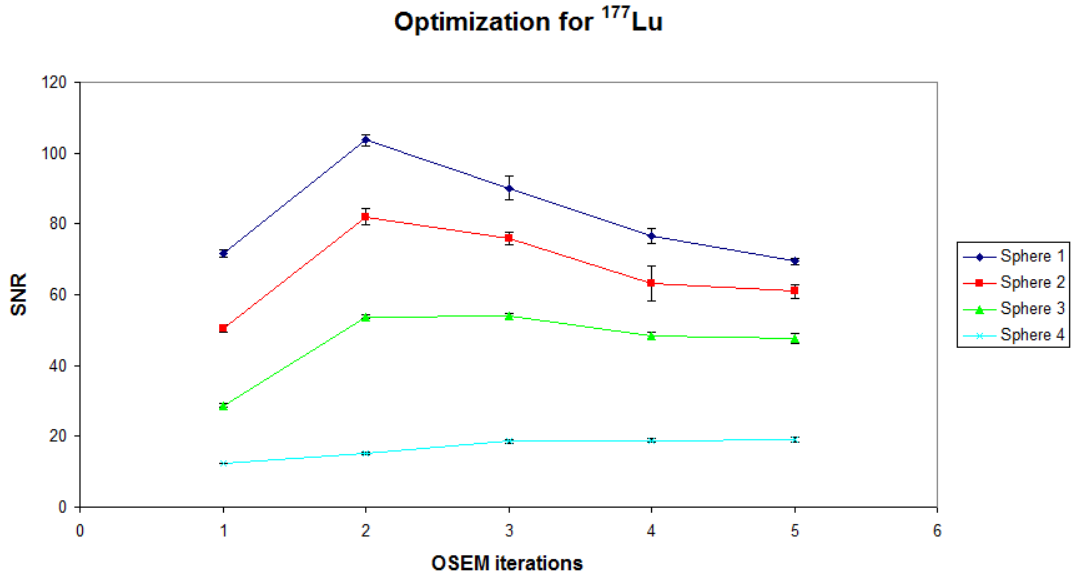

Figure 19: SNR plotted as a function of OSEM iterations with ten subsets for the NEMA-phantom with ^{177}Lu applied on a Lutetium protocol using the ELEGP collimator. Sphere 1 is the largest sphere and Sphere 4 is the fourth largest sphere. The error bars indicate SEM.

To compare the two collimators, contrast was plotted as a function of noise in Figure 20. The graphs show that the contrast was higher using the MEGP collimator compared to the ELEGP collimator.

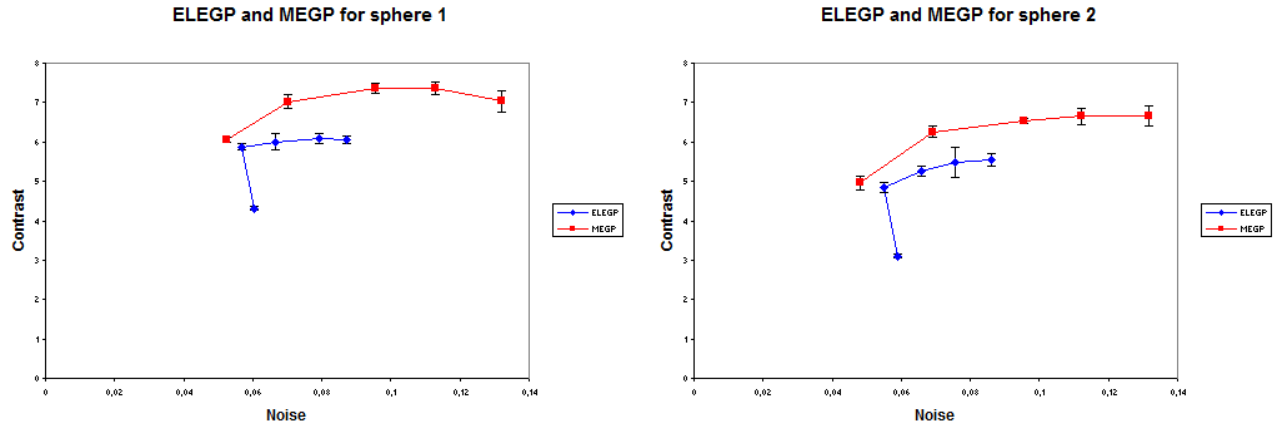

Figure 20: Contrast plotted as a function of noise for one to five OSEM iterations for A: sphere 1 and B: sphere 2. The collimators shown are both ELEGP and MEGP and the nuclide used is ^{177}Lu. The five noise levels were generated with one to five OSEM iterations with ten subsets. The lowest noise level for the ELEGP collimator was generated with two OSEM iterations. The second lowest noise level with the ELEGP collimator is generated with one OSEM iteration and the noise then increased with an increased number of itarations up to five OSEM iterations. For the MEGP collimator, the noise increased with an increased number of iterations. The error bars displays SEM.

The contrast and noise were also compared for sphere 3 and 4 (Figure 21). The difference in contrast was smaller for sphere 4 for both collimators compared to the other spheres. The SNR was lower for the ELEGP collimator for the most relevant iteration steps compared to the MEGP collimator.

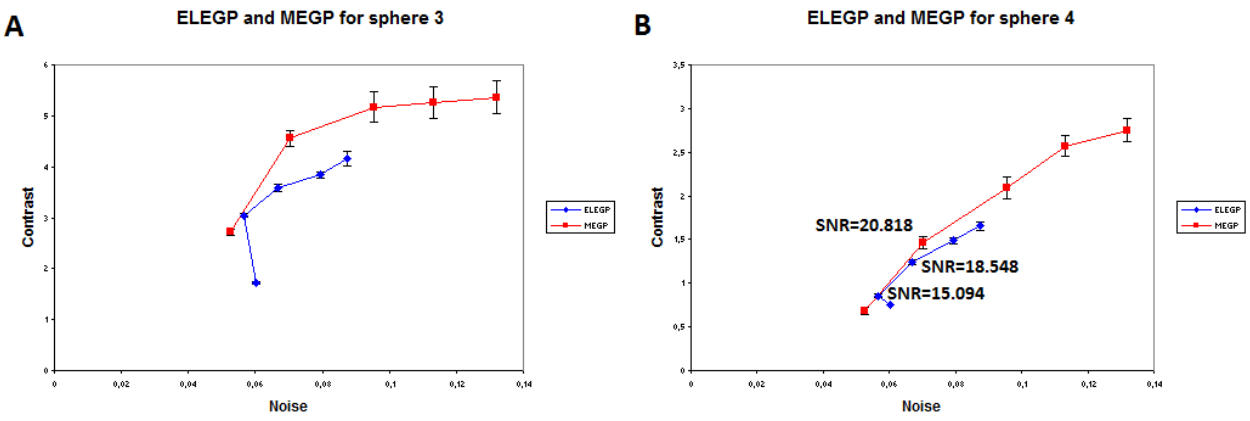

Figure 21: Contrast plotted as a function of noise for one to five OSEM iterations for A: sphere 3 and B: sphere 4. The collimators shown are both ELEGP and MEGP and the nuclide used is ^{177}Lu. The five noise levels are generated with one to five OSEM iterations with ten subsets. The lowest noise level for the ELEGP collimator is generated with two OSEM iterations. The second lowest noise level with the ELEGP collimator is generated with one OSEM iteration and the noise then increased with an increased number of itarations up to five OSEM iterations. For the MEGP collimator, the noise increased with an increased number of iterations. The error bars displays SEM. The SNR is displayed for the most relevant iteration steps.

Images with the highest SNR for both collimators are displayed in Figure 22.

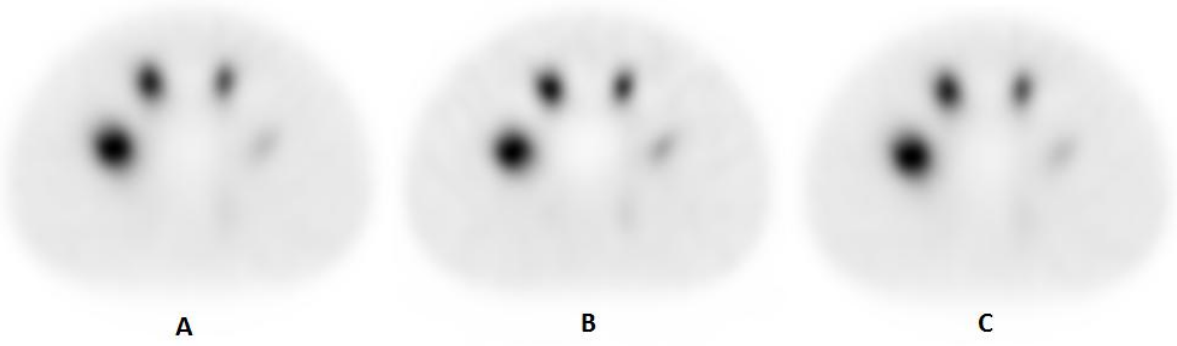

Figure 22: Images of the NEMA phantom with the highest SNR for both collimators using a protocol for ^{177}Lu. A: Two OSEM iterations and ten subsets with the ELEGP collimator. B: Three OSEM iterations and ten subsets with the ELEGP collimator. C: Two OSEM iterations and ten subsets with the MEGP collimator (used clinically).

Discussion

The purpose of this study was to investigate SPECT/CT images acquired using the ELEGP collimator reconstructed with resolution recovery (Evolution®) and compare it to the traditionally used collimator for the four supported nuclides. A reconstruction modelling CDR could make it possible to redesign the collimator (exchange LEHR or MEGP to ELEGP collimators) to gain sensitivity, less noise and preserve image contrast. According to vendor's documentations, Xeleris 3.1 and Evolution Toolkit supports reconstruction using the Evolution algorithm to reconstruct images acquired with the ELEGP collimator for the following radionuclides; ^{99m}Tc, ^{111}In, ^{123}I and ^{177}Lu (^{111}In and ^{177}Lu will work but are not validated).

Reconstructions with two iterations and ten subsets gave the highest SNR when acquiring ^{99m}Tc, ^{111}In, ^{123}I and ^{177}Lu images with the NEMA phantom for the ELEGP collimator. It was not of interest to analyse images over five OSEM iterations since these images had very high noise levels and low SNR. Optimally 1 to 50 equivalent MLEM iterations would be analysed but due to the limited time for this study ten subsets was used while the impact of different numbers of iterations was studied. Ten subsets were chosen since it is clinically used at Sahlgrenska University hospital.

Contrast versus noise in images acquired with ELEGP collimator, ^{99m}Tc and ^{123}I (Figure 6, 7, 14 and 15) shows that for every measured noise level the contrast was higher for the ELEGP collimator compared to the LEHR collimator. Increased contrast for ^{123}I-imaging could be due to less septum penetration in the ELEGP collimator. To properly compare the two collimators, reconstruction of different numbers of iterations for the ELEGP collimator was compared to the reconstruction with two iterations for the LEHR collimator; which is the clinical standard procedure. The analysis of contrast versus noise levels for ^{111}In and ^{177}Lu (Figure 10, 11, 18 and 19) showed that for every chosen noise level the contrast was lower for the ELEGP collimator compared to the MEGP collimator for all spheres, which contradicts earlier published results for ^{111}In [4]. However, the reconstructions in the previous study were not performed with Evolution™ toolkit, an alternative non-commercial software was used. The difference in results could be because Evolution™ toolkit does not use corrections for septum scatter or septum penetration for ELEGP unlike the software in the other study. The difference could also be due to the difference in ROI placement; in this study the ROI was placed at FWHM for the sphere signal, but in the study done by Mahler et al [4] the ROI was placed at a fixed size for every sphere. If the optimal number of iterations for both collimators are compared, the ELEGP collimator was inferior in SNR for all spheres investigated. This could be due to the high energy of ^{111}In and septum penetration which would lower the contrast. For ^{111}In and ^{177}Lu, one iteration for ELEGP collimator gave a higher noise level than a two iteration reconstruction, Figure 11. This was probably because of the low spatial resolution of the spheres for these measurements, which leads to the spheres contributing to the background ROIs.

The smaller spheres are the most important to observe when optimizing SNR, since these are the most challenging to detect clinically. The tumour size detection limit is dependent on the location of the tumour, clinical relevant activity concentrations in hot-spots vs. background, and isotope [10]. Sphere 3 with a diameter of 22 mm is the smallest sphere in the NEMA-phantom that could be analysed for ^{99m}Tc-bone scintigraphy due to the sphere signal drowning in the high background activity for smaller spheres. The clinical detection limit for ^{99m}Tc-bone scintigraphy is however at about 15 mm in diameter [11]. The detection limit for ^{111}In is about 20 mm wide depending on tumour location and uptake which is similar to the size of sphere 3 in the NEMA phantom. E.g. small bowel neuroendocrine tumours (SBNET) smaller than 20 mm are hard to detect due to an uptake only 2-4 fold greater than the background [11]. Sphere 4 (17 mm in diameter) on the other hand is the most clinically sized sphere compared to nodules imaged with ^{123}I-DaTSCAN™. The average detection limit for ^{177}Lu is at about 17mm diameter aswell.

The most optimal number of iterations for ^{99m}Tc reconstructions with the ELEGP collimator are two and three. If using two iterations the contrast was lower compared to the LEHR collimator but the noise level and the overall SNR was better. If three iterations for the ELEGP collimator was chosen, the contrast was similar as for two iterations using a LEHR collimator but the noise was lower. There is still a possibility that the difference between ELEGP and LEHR in this case is even smaller for tumours closer to the detection limit. This is indicated by the trend of decreasing difference in contrast for sphere 1 to 3. Figure 9 shows that the most optimal iteration for ^{111}In is two iterations. When reconstructions with two iterations for both collimators are compared, Figure 11 shows that the noise and contrast are lower for the ELEGP and that the SNR is similar for both collimators. Figure 13 shows that three or more iterations were optimal in terms of SNR for ^{123}I-DaTSCAN™ with sphere 4 (the clinically relevant sphere). Two iterations was still the best choice, because of the high SNR for sphere 2 and 3. If two iteration reconstructions for both collimators was compared for sphere 4 it can be seen that the ELEGP collimator images have a lower noise level and contrast but a higher overall SNR, Figure 15. With three iterations and ELEGP collimator, the contrast is higher too. For larger spheres, the ELEGP collimator was superior. The most optimal number of iterations for ^{177}Lu was two and three, Figure 17. If these steps are compared to the second iteration step for the MEGP collimator in Figure 19B, it can be seen that the SNR is lower for the ELEGP collimator.

For ^{123}I artificial Poisson noise was added to image raw data acquired with the ELEGP collimator, and reconstructed with two iterations. Noise was added until the SNR in sphere 4 (most relevant sphere clinically) matched the SNR found in reconstructions with two iterations for the LEHR collimator. This was only done with ^{123}I because this was the only nuclide which showed better SNR for spheres with clinically relevant sizes. The results showed that Poisson noise which corresponded to 50% of the total acquisition time could be added to the image before the SNR matched. This means that half of the scan time could be saved by using the ELEGP collimator instead of the LEHR collimator.

Using a physical phantom and detectors has an advantage over simulated acquisitions and images, since it is closer to a realistic scenario. An advantage with the NEMA-phantom used in this study was that spheres with different sizes could be evaluated in one acquisition. A drawback is the lack of statistics by not using a phantom where the spheres are the same size.

There are also some disadvantages not using simulation such as more sources of error and not being able to measure as many times for better statistics. A source of error in this study was to find a representable ratio between the background to sphere ratio by looking at patient images since the uptake and background differed within and between patients. Another source of error was when filling the phantom with activity. It was difficult to get the real ratio between background and spheres. This study could have been done differently by analysing a higher number of patient images. The ratio between background and hot-spots fluctuated to a high degree between the clinical images, and more ratios should have been analysed to get a more correct ratio between background and hot-spots. All these sources of error will lead to the ratio between background and sphere activity to deviate some from clinical situations. This error will not matter to any great extent since this ratio was an approximation to begin with.

For patient images, a couple of approximations were made; the background was approximated having a homogeneous activity distribution and the tumours were approximated with a sphere. The attenuation was also approximated with attenuation in water. Other sources of error were when adding artificial noise and the method used for ROI placement. Depending on how the ROI is placed, the average count can vary (Figure 4). An error could also be the assumption that activity could perfectly be compensated for with imaging time. This may necessarily not be true.

In this study, SNR was used to a great extent to describe image quality. The type of SNR used in this study can be an incomplete tool to describe image quality since among others it does not fully describe what an actual human observer can detect in an image. Noise and contrast levels may have varying importance in different images; this cannot be described by SNR. Some of the problem with SNR was

avoided in this study by comparing contrast and noise from different collimators separately. If both the contrast and the noise levels was better in an image, it would have been a better indicator that the image was superior. Describing noise with the method used in this study is also a problem when the noise is not uncorrelated and the type of noise differs between images, which is the case for this study. The type of noise differs both between different collimators and different numbers of OSEM iterations. The reason why quantification was not tested in this study was because it is rarely used clinically with these examinations and it is not a trivial thing to do due to the non-linear nature of model based compensation. Different post filters were not tested because they are not used to any great extent at Sahlgrenska University hospital.

Several tasks needs to be investigated related to this study. All the reconstructions in this study were done with CT for attenuation correction. CT is not always used clinically with SPECT and reconstructed images without CT are of interest to be analysed. To optimize the images further, a higher number of equivalent MLEM iterations with OSEM could be tested to find out the optimal iteration number with higher accuracy. Filters were not used in this study, this could also be experimented with. The difference between the uptakes in hot-spots in the patient varied a lot for the same examination and the ELEGP could be tested for different hot-spot locations, sizes and types. To save some acquisition time, 60 projections could be tested instead of 120 projections [5]. Another way to evaluate image quality is to use visual grading. This is more time consuming but can be a good complement to this study [12].

Conclusion

In this study, we demonstrated that ELEGP collimator is superior to the clinically used LEHR collimator for ^{123}I and ^{99m}Tc. ^{123}I was shown to work very well with the ELEGP collimator and could reduce scan times by 50% compared to scans with the LEHR collimator. We therefore propose that the ELEGP collimator is used in the clinic for examinations using ^{123}I. Imaging ^{99m}Tc with the ELEGP collimator should be investigated further. According to these results the ELEGP collimator cannot be recommended for ^{111}In and ^{177}Lu, it did not perform as well as in other studies [1-4]. This could be due to Evolution Toolkit® not supporting model based compensation for septum penetration and collimator scatter for the ELEGP collimator. The performance of the ELEGP collimator with RR should be investigated further.

Reference list

1. Carlsson S, Svensson SE. Nuklearmedicin. Fysik & teknik, radiofarmaka, nuklearmedicinska bilder, datoranvändning, spårämneskinetik, strålrisker & strålskydd, kvalitetssäkring [Internet]. Stockholm: Svensk förening för nuklearmedicin. 2007 Oct. Available at: http://www.sfnm.se/wp/wp-content/uploads/2013/08/Nuklearmedicin_SC_SES.pdf

2. Radioisotopes in medicine [Internet]. World nuclear association. 2015. Available at: http://www.world-nuclear.org/information-library/non-power-nuclear-applications/radioisotopes-research/radioisotopes-in-medicine.aspx

3. Evolution for bone™ collimator-detector response compensation in iterative SPECT imaging reconstruction algorithm [Whitepaper]. Version 1.0. GE Healthcare Waukesha, WI U.S.A. 2005 General Electric Company.

4. Mahler E, Sundstrom T, Axelsson J, Larsson A. Detecting small liver tumors with In-111-pentetreotide SPECT-a collimator study based on monte carlo simulations. Ieee transactions on nuclear science. 2012;59(1):47-53.

5. Holmberg D. Optimisation of image acquisition and reconstruction of 111In-pentetrotide SPECT [Master thesis]. Umeå university Sweden, Department of radiation sciences. 2012.

6. Mähler E. Optimering av bildkvaliteten för SPECT-undersökningar med 111In-Octreoscan vid Norrlands universitetssjukhus:-en monte carlo studie [Master thesis]. Umeå university Sweden, Department of radiation sciences. 2011.

7. Larsson A. Corrections for improved quantitative accuracy in SPECT and planar scintigraphic imaging [Dissertation]. Umeå university Sweden, Department of radiation sciences. Print & media. 2005.

8. Bruyant PP. Analytic and iterative reconstruction algorithms in SPECT. Journal of nuclear medicine. 2002;43(10):1343-58.

9. King MA, Glick SJ, Pretorius PH, Wells RG, Gifford HC, Narayanan MV. Attenuation, scatter, and spatial resolution compensation in SPECT. Emission tomography academic press-The fundamentals of PET and SPECT, Amsterdam, The Netherlands: Elsevier academic press; 2004:74–89

10. Erdi YE. Limits of Tumor Detectability in Nuclear Medicine and PET. Molecular imaging and radionuclide therapy. 2012;21(1):23.

11. Maxwell JE, Sherman SK, Menda Y, Wang D, O'Dorisio TM, Howe JR. Limitations of somatostatin scintigraphy in primary small bowel neuroendocrine tumors. Journal of surgical research. 2014;190(2):548-53.

12. L.G. Månsson Methods for the Evaluation of Image Quality: A Review. Radiation protection dosimetry. 2000;90(1-2):89-99.